TESTING GENERAL RELATIVITY

Constraints on the number of spacetime dimensions using gravitational wave detections

Meryl Kinnear, November 14, 2021[1]

[1] *University of Glasgow*

ABSTRACT

This investigation uses gravitational wave events GW170817 and GW190521 along with their proposed electromagnetic counterparts to place bounds on the number of non-compact spacetime dimensions through which gravity propagates. The assumption that in a D-dimensional universe, short-wavelength photons move through 3 spatial dimensions whilst long-wavelength gravitational waves propagate through $D-1$, allows the relationship between the inferred distances to be characterised by a gravitational leakage (friction) parameter. Constraints are attained via Bayesian inference using three different gravitational waveform models and two sets of cosmological constants from the Planck collaboration and $\mathrm{SH_0ES}$. The number of dimensions is found to be consistent with $(3+1)$-dimensional general relativity at a significance level of 0.1 for the combined events in all cases. This sees an improvement in lower bounds by a factor of ~ 2 compared to previous studies using only GW170817. A deviation from general relativity at this level in the GW190521-only results is observed and several explanations are proposed, including possible $(4+1)$-dimensional modified gravity scenarios, but no formal conclusions can be drawn. Future gravitational wave observation missions such as LISA will vastly improve the ability of similar studies to place constraints on the number of dimensions and other general relativity deviation parameters.

1. INTRODUCTION & BACKGROUND

1.1. *General Relativity & Higher-Dimensional Theories*

Albert Einstein's general theory of relativity (GR) [24] is the theory that gravitation is a geometric property of spacetime. As Wheeler [54] put it,"spacetime tells matter how to move; matter tells spacetime how to curve." It is a very elegant and overall successful model of gravitation, having been confirmed by numerous [55] experimental [51] and observational [23, 45] tests in both the strong and weak field regimes. However, it would appear that GR is incomplete as there are some problems that the theory fails to solve: the hierarchy problem [36] (why is gravity "weaker" than the other fundamental forces?), the Hubble tension [30] (why do the measurements of H_0 for early and late universe disagree?), and dark energy [44, 48] (what is causing the rate of expansion of the universe to increase?). This has led to a number of theories of modified gravity that seek to expand GR and explain these phenomena [16].

A consequence of Lovelock's theorem [38] is that metric theories of gravity that differ from GR must fall into one of five categories: alternative field, higher-order metric derivative, higher-dimensional, non-local and emergent. The subset of theories relevant to this discussion are higher-dimensional theories[1]. That is, models where the standard 4-dimensional mathematical framework of GR is expanded into 5 or more non-compact[2] dimensions. For example, one family of these theories is called Braneworld models (e.g. the DGP model [22]), where the universe is described as a 3-dimensional surface (a brane) embedded in a 5 (or more) dimensional Minkowski space called a bulk.

There are a number of tests of modified gravity, but one emerging field of astrophysics provides a unique tool for the study of gravitation: gravitational wave astronomy. The existence of gravitational radiation is predicted by GR, in the form of quadrupole transverse waves, as the free-space solutions to Einstein's field equations in linearised gravity. These gravitational waves (GWs) are generated by any non-spherically-symmetric acceleration of matter. The effect is negligible in most scenarios, but a number of compact massive binary merger events have now (as of 2015) successfully been detected as strain in ground based Michelson interferometers [2, 9]. Information about the number of dimensions is encoded in these signals, in the polarisation, propagation velocity and luminosity distance.

1.2. *Gravitational Waves*

On the 17th of August 2017 the first binary neutron star (BNS) merger was detected by the Laser Interferometer Gravitational-Wave Observatory, LIGO [6]. An advantage of BNS events over binary black hole (BBH) mergers is that the merger itself produces electromagnetic (EM) radiation in the form of a gamma ray burst (GRB), to which GW170817 is no exception. The 2 second long GRB was detected by Fermi [52] in a galaxy $\sim$ 40 Mpc away, 1.7 seconds after the GW signal. This event ushered in a new era of multi-messenger astronomy as such events provide astronomers with the means to independently measure two fundamentally different forms of radiation from a single source. The associated multi-messenger astronomy paper "Multi-messenger Observations of a Binary Neutron Star Merger"—Abbott et al. [1], is a collaboration between over 50 teams of GW, EM and neutrino astronomers.

To date, there has been one[3] confirmed EM counterpart to a GW detection and one proposed counterpart. The first event, GW170817 [6] is a BNS merger with counterpart gamma ray burst GRB 170817A [52]. The second event is GW190521 [10], not a BNS but a BBH which coincided with an EM 'flash' which is speculated [31] to have been caused by the resulting black hole being thrown through the accretion disk of a nearby supermassive black hole by merger recoil.

[1] See 'Cosmology and Modified Gravity' by Clifton et al. [19] for a comprehensive review of alternative theories of gravitation.

[2] Distinct from the compactified dimensions described in string theory, which are of finite length and not of interest here.

[3] Another BNS, GW190425 was detected by LIGO Livingston but no EM counterpart has been confirmed so it will not be discussed in this report.

Gravitational wave events, with and without EM counterparts, can be utilised in various ways to constrain GR and alternative theories [3]. The phase evolution of the GW signals can be described by a set of coefficients modified by post Newtonian parameters. This allows for parameterisation of deviations from GR and is the main method used to test GR with GWs, but other signal characteristics such as polarisation and luminosity distance can be assessed [4]. In all tests so far, the results have been found to agree very well with general relativity [3].

One of the great benefits of GW detections is that the luminosity distance information is encoded entirely in the amplitude of the signal [50]:

$$h_{+\times}(t) \propto \frac{[(1+z)\mathcal{M}]^{5/3}\, f(t)^{2/3}}{d_{\mathrm{L}}}. \tag{1.1}$$

Here $h_{+\times}$ is the time domain strain measured by the interferometer in the event of a passing GW, f is the frequency, z is the redshift and d_{L} is the luminosity distance of the source. The chirp mass, $\mathcal{M}$ is a function of masses of the two merging bodies, defined as,

$$\mathcal{M} = \frac{(m_1 m_2)^{3/5}}{(m_1+m_2)^{1/5}}. \tag{1.2}$$

Since the time derivative of the frequency, $\dot{f}$ scales as a function of z, $\mathcal{M}$ and f, but not d_{L},

$$\dot{f}(t) \propto [(1+z)\mathcal{M}]^{5/3}\, f(t)^{11/3}, \tag{1.3}$$

the luminosity distance can be measured from the amplitude, independently of the other parameters. This has earned GW events the title of "standard sirens", analogously to "standard candles". That is, the distance can be directly inferred from the observation.

There are several papers that offer discussion about how this attribute could be used [18, 50] and has been used [5, 8, 28] to measure the Hubble constant, H_0, independently of measurements from supernovae (Riess et al. [47], hereafter $\mathrm{SH_0ES}$) and CMBR polarisations (Aghanim et al. [12], the Planck Collaboration), although the precision is not yet on par with these other methods. The techniques used here, and in Pardo et al. [43] and Mastrogiovanni et al. [40], for constraining the number of dimensions are largely similar to the ones used to provide constraints on H_0 in that they essentially create a model of the gravitational wave luminosity distance as a function of the parameters of interest and compare it to the GW-measured distance.

1.3. *The Gravitational Leakage Parameter*

The effect of extra dimensions on GWs can be thought of as a systematic error on the luminosity distance, causing GW sources to appear further away than they actually are. This "error" can be parameterised as follows. As shown above, in 4-dimensional GR, the amplitude of a gravitational wave signal is inversely proportional

to its luminosity distance, $d_{\rm L}^{\rm GW}$:

$$h_{+\times}(t) \propto \frac{1}{d_{\rm L}^{\rm GW}}. \tag{1.4}$$

However, when considering a D-dimensional GR expansion such as the DGP model, conservation of flux over the $(D-1)$-dimensional hyper sphere centered at the source requires that the amplitude scales with a "true" luminosity distance, $d_{\rm L}$ as [21],

$$h_{+\times}(t) \propto \frac{1}{d_{\rm L}\left[1+\left(\frac{d_{\rm L}}{R_{\rm c}}\right)^{n(\gamma-1)}\right]^{1/n}} \tag{1.5}$$

where $R_{\rm c}$ is the crossover scale, beyond which gravity begins to exhibit gravitational leakage, n is the steepness of the transition, and γ[4] is the gravitational leakage parameter, defined as[5]:

$$\gamma = \frac{D-2}{2}. \tag{1.6}$$

For $R_{\rm c} \ll d_{\rm L}$, Equation 1.5 simplifies to,

$$h_{+\times}(t) \propto \frac{1}{(d_{\rm L})^{\gamma}}. \tag{1.7}$$

Thus, combining 1.4 and 1.7, $d_{\rm L}$ can be related to the GR assumed luminosity distance by,

$$d_{\rm L} = \left(d_{\rm L}^{\rm GW}\right)^{1/\gamma}. \tag{1.8}$$

The Friedmann–Lemaître–Robertson–Walker metric provides a solution to Einstein's field equations corresponding to an isotropic, homogeneous universe. From this metric, the Friedmann equation can be derived. The Friedmann equation describes the evolution of the geometry of the universe and can be expressed in the simplified form:

$$\left(\frac{H}{H_0}\right)^2 = \Omega_{\rm rad}(1+z)^4 + \Omega_{\rm m}(1+z)^3 + \Omega_{\rm k}(1+z)^2 + \Omega_{\Lambda}, \tag{1.9}$$

which allows the cosmological model to be described by the Hubble parameter, H, the Hubble constant, $H_0 \coloneqq H|_{t_0}$, and a set of dimensionless present-day[6] cosmological density parameters corresponding to: radiation energy density, $\Omega_{\rm rad}$, total matter density, $\Omega_{\rm m}$, the curvature parameter, $\Omega_{\rm k}$, and "dark" energy density Ω_{Λ}. Both Planck and $\rm SH_0ES$ provide strong evidence that suggests the universe is flat ($k = \Omega_{\rm k} = 0$) and that $\Omega_{\rm rad}$ is sufficiently close to 0 that the approximation $\Omega_{\Lambda} = 1 - \Omega_{\rm m}$ can

[4] This γ notation is borrowed from Pardo et al. [43] and is simply to prevent the untidiness caused by writing indices in D explicitly.

[5] Note that $\gamma = 1$ corresponds to $D = (3+1)$.

[6] The usual convention is that, for example, $\Omega_{\rm m}$ refers to the time-varying parameter and $\Omega_{\rm m,0} \coloneqq \Omega_{\rm m}|_{t_0}$. In this text, for notational convenience, the subscript 0 has been dropped since density parameters are *always* referring to their present-day values, $\Omega_{\rm m} \equiv \Omega_{\rm m,0}$.

be made. So, for a set of cosmological parameters such that $(\Omega_{\rm rad}, \Omega_{\rm m}, \Omega_{\rm k}, \Omega_\Lambda) = (0, \Omega_{\rm m}, 0, 1-\Omega_{\rm m})$, the function $E(z)$ defined by:

$$E(z) \coloneqq \frac{H}{H_0} = \sqrt{\Omega_{\rm rad}(1+z)^4 + \Omega_{\rm m}(1+z)^3 + \Omega_{\rm k}(1+z)^2 + \Omega_\Lambda}, \tag{1.10}$$

simplifies to,

$$E(z) = \sqrt{\Omega_{\rm m}(1+z)^3 - \Omega_{\rm m} + 1}, \tag{1.11}$$

which is the expression used for $E(z)$ throughout this analysis.

The luminosity distance of a source in a flat universe can now be related to its redshift z by:

$$d_{\rm L} = (1+z)d_{\rm C} = (1+z)\frac{c}{H_0}\int_0^z \frac{1}{E(z')}{\rm d}z', \tag{1.12}$$

where c is the speed of light in km s^{-1} and z' is a dummy parameter used for integration. The comoving distance $d_{\rm C}$, is the distance between two points in comoving coordinates, i.e. a coordinate system that is expanding with the universe. The idea of comoving volume $V_{\rm C}$ arises somewhat frequently in this paper, particularly in Section 2.1, and in a flat universe is simply the volume of the sphere with radius $d_{\rm C}$ [33].

The aim of this work is to test GR by using Bayesian inference to place bounds on the number of spacetime dimensions through which gravity propagates. Luminosity distance measurements from gravitational wave events GW170817 and GW190521 are compared via Equation 1.8 to their true luminosity distances, calculated from EM-measured redshifts of their host galaxies using Equation 1.12. Section 2 details the derivation of the likelihood function used to infer the leakage parameter, preparation of the GW and EM data, including sample selection, and an outline of the stochastic sampling method. The results of the parameter estimation are presented in Section 3 followed by a discussion of their significance and relation to future research in Section 4.

2. METHOD

The core idea of the approach of this investigation is to construct a model of $d_{\rm L}^{\rm GW}$ with respect to z, γ, H_0 and $\Omega_{\rm m}$ and evaluate the likelihood, the conditional probability of obtaining a set of GW and EM data given a set of parameter values, $p(x_{\rm GW}, x_{\rm EM}|\gamma, z, H_0, \Omega_{\rm m})$. This is then multiplied by a prior on each parameter to obtain a posterior, $p(\gamma, z, H_0, \Omega_{\rm m}|x_{\rm GW}, x_{\rm EM})$, which can be marginalised over all other parameters and normalised to obtain a posterior distribution for γ, $p(\gamma|x_{\rm GW}, x_{\rm EM})$. The method used here can be considered an expansion of the one used in Pardo et al. [43] which relies heavily on the work of Deffayet & Menou [21]. In addition to the relatively nearby (∼40 Mpc) event GW170817, discussed in Pardo et al. [43], this analysis is performed on GW190521 which is considerably further away (∼3000–6000 Mpc). Thus, since the methods used in Pardo et al. [43] make many assumptions based on approximations valid only in the nearby universe, it must be generalised to account for non-Euclidean cosmology.

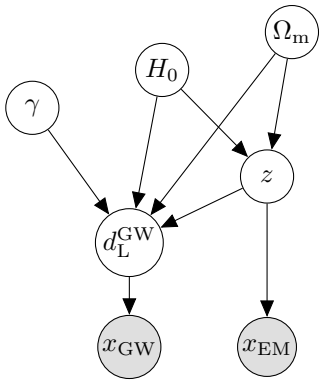

Figure 1. A graphical representation of the statistical relationships between parameters and observed data. Filled nodes represent observables and open nodes are inferred parameters which require priors. The arrows indicate a statistical dependency; e.g. the measured GW data, $x_{\rm GW}$, depends on the luminosity distance of the source, $d_{\rm L}^{\rm GW}$.

In order to avoid having to account for selection effects [37, 39], the likelihood function is derived on the premise that the analysis can be performed such that a model of z is constructed from $d_{\rm L}^{\rm GW}, \gamma, H_0, \Omega_{\rm m}$ (i.e. the direction of the arrow from z to $d_{\rm L}^{\rm GW}$ in Figure 1 is reversed) and then a change of variables is performed to allow for sampling in z. The full derivation, with justifications, is detailed in Section 2.1. Sections 2.2 and 2.3 describe the prior distributions, and sources of the GW and EM data used in the posterior function. The resulting posterior distribution is approximated using stochastic sampling techniques as described in Section 2.4.

2.1. *Statistical Framework*

In this section, the "hat' notation ($\hat{\cdot}$) denotes a function. It is assumed that the GW detections and their corresponding EM counterparts do indeed originate from the same source and further, that the EM and GW distance measurements are independent of one another. Therefore, the likelihood of observing some gravitational wave data $x_{\rm GW}$, and electromagnetic observation data $x_{\rm EM}$, given γ, $d_{\rm L}^{\rm GW}$, z, H_0 and $\Omega_{\rm m}$, can be factorised as:

$$p(x_{\rm GW}, x_{\rm EM}|\gamma, d_{\rm L}^{\rm GW}, z, H_0, \Omega_{\rm m}) = p(x_{\rm GW}|d_{\rm L}^{\rm GW})p(x_{\rm EM}|z). \tag{2.1}$$

Here $x_{\rm GW}$ and $x_{\rm EM}$ are not directly dependent on γ, H_0 and $\Omega_{\rm m}$, as shown in Figure 1, and so arise in the priors for $d_{\rm L}^{\rm GW}$ and z but not in the likelihoods. It follows from Bayes theorem that the posterior probability is proportional to the likelihood multiplied by prior probability:

$$p(\gamma, d_{\rm L}^{\rm GW}, z, H_0, \Omega_{\rm m}|x_{\rm GW}, x_{\rm EM}) \propto p(x_{\rm GW}|d_{\rm L}^{\rm GW})p(x_{\rm EM}|z)p(\gamma, d_{\rm L}^{\rm GW}, z, H_0, \Omega_{\rm m}). \tag{2.2}$$

Marginalising over all other parameters gives the posterior distribution for γ:

$$p(\gamma|x_{\rm GW}, x_{\rm EM}) = \frac{1}{\beta(\gamma)} \iiiint p(x_{\rm GW}|d_{\rm L}^{\rm GW})p(x_{\rm EM}|z) \\ p(\gamma, d_{\rm L}^{\rm GW}, z, H_0, \Omega_{\rm m}) {\rm d}d_{\rm L}^{\rm GW} {\rm d}z {\rm d}H_0 {\rm d}\Omega_{\rm m}, \tag{2.3}$$

where β is the normalisation factor (see below).

Now, this expression can be simplified in several ways. Firstly, the need to to integrate over z can be removed by modelling z as a function of the other parameters, then some assumptions can be applied to show that β is constant with respect to γ and hence can be neglected. Consider the GR-assumed luminosity distance, $d_{\rm L}^{\rm GW}$, related to z by Equations 1.8 and 1.12. This can be expressed as a function, $\hat{d}_{\rm L}^{\rm GW}$, such that,

$$\hat{d}_{\rm L}^{\rm GW}(z,\gamma,H_0,\Omega_{\rm m}) = \left[(1+z)\frac{c}{H_0}\int_0^z \frac{1}{E(z',\Omega_{\rm m})}{\rm d}z'\right]^{\gamma}. \tag{2.4}$$

This is bijective for $z > 0$, so $\hat{d}_{\rm L}^{\rm GW}$ is invertible with respect to z and has inverse $\hat{z}$. Here it has been assumed that for both events $R_{\rm c} \ll d_{\rm L}$, that is, the screening scale of any extra dimensions is much less than the distance of the events so that gravitational leakage would have an effect on the signals described in Equation 1.7. This is discussed further in Section 4. It is also assumed that the luminosity distance obtained from EM data is the true luminosity distance of the source, i.e. there is no gravitational leakage experienced by photons [22]. Now, in the case that z is dependent on $d_{\rm L}^{\rm GW}$ and therefore γ, the priors can be factorised as,

$$p(\gamma, d_{\rm L}^{\rm GW}, z, H_0, \Omega_{\rm m}) = p(\gamma)p(d_{\rm L}^{\rm GW}|H_0,\Omega_{\rm m})p(z|d_{\rm L}^{\rm GW},\gamma,H_0,\Omega_{\rm m})p(H_0)p(\Omega_{\rm m}), \tag{2.5}$$

and since the parameter z is dependent on $d_{\rm L}^{\rm GW},\gamma,H_0,\Omega_{\rm m}$, it can be factored out by approximating the prior as a Dirac delta function. i.e.,

$$p(z|d_{\rm L}^{\rm GW},\gamma,H_0,\Omega_{\rm m}) = \delta(z-\hat{z}(d_{\rm L}^{\rm GW},\gamma,H_0,\Omega_{\rm m})), \tag{2.6}$$

and,

$$\int p(x_{\rm EM}|z)\delta(z-\hat{z}(d_{\rm L}^{\rm GW},\gamma,H_0,\Omega_{\rm m})){\rm d}z = p(x_{\rm EM}|\hat{z}(d_{\rm L}^{\rm GW},\gamma,H_0,\Omega_{\rm m})). \tag{2.7}$$

Now Equation 2.3 is equal to:

$$\frac{1}{\beta(\gamma)}\iiint p(x_{\rm GW}|d_{\rm L}^{\rm GW})p(x_{\rm EM}|\hat{z}(d_{\rm L}^{\rm GW},\gamma,H_0,\Omega_{\rm m})) \\ p(d_{\rm L}^{\rm GW}|H_0,\Omega_{\rm m})p(\gamma)p(H_0)p(\Omega_{\rm m}){\rm d}d_{\rm L}^{\rm GW}{\rm d}H_0{\rm d}\Omega_{\rm m}. \tag{2.8}$$

The normalisation factor encodes the selection effects and ensures that the posterior integrates to 1. Selection effects account for bias introduced due to the limits of the detectors. For example, the luminosity distances of a population of events might be underestimated if the most distant sources are not detected. Here, the normalisation factor is given by[7]:

$$\beta(\gamma) = \iiint_0^{d_{\rm max}} P_{\rm det}^{\rm GW}(d_{\rm L}^{\rm GW})P_{\rm det}^{\rm EM}(\hat{z}(d_{\rm L}^{\rm GW},\gamma,H_0,\Omega_{\rm m})) \\ p(d_{\rm L}^{\rm GW}|H_0,\Omega_{\rm m})p(H_0)p(\Omega_{\rm m}){\rm d}d_{\rm L}^{\rm GW}{\rm d}H_0{\rm d}\Omega_{\rm m}, \tag{2.9}$$

[7] See Loredo [37] and Mandel et al. [39].

where $d_{\rm max}$ is the maximum distance a GW source could be detected for the sensitivity of detectors at the time of the detection. The detection probability, $P_{\rm det}$ is the probability that a signal with some set of parameters could be detected. Following Abbott et al. [5], the assumption can be made that at the required distances, an EM signal can always be detected so $P_{\rm det}^{\rm EM} = 1$, and the other factors are constant with respect to γ so, assuming a mass prior independent of z (and hence $d_{\rm max}$ independent of z), β can be dropped since it is a constant[8]. This leaves:

$$p(\gamma|x_{\rm GW}, x_{\rm EM}) \propto \iiint p(x_{\rm GW}|d_{\rm L}^{\rm GW}) p(x_{\rm EM}|\hat{z}(d_{\rm L}^{\rm GW}, \gamma, H_0, \Omega_{\rm m})) \\ p(d_{\rm L}^{\rm GW}|H_0, \Omega_{\rm m}) p(\gamma) p(H_0) p(\Omega_{\rm m}) {\rm d}d_{\rm L}^{\rm GW} {\rm d}H_0 {\rm d}\Omega_{\rm m}. \quad (2.10)$$

In order to perform the posterior sampling on this function, a change of variables must be applied to allow $d_{\rm L}^{\rm GW}$ to be written as a function of z [9]. For any function $f(d_{\rm L}^{\rm GW})$, the integral over $d_{\rm L}^{\rm GW}$ is given by,

$$\int f(d_{\rm L}^{\rm GW}) {\rm d}d_{\rm L}^{\rm GW} = \int f(\hat{d}_{\rm L}^{\rm GW}(z)) \left|\det(\mathbf{J}_d(z))\right| {\rm d}z = \int f(\hat{d}_{\rm L}^{\rm GW}(z)) \left|\frac{\partial d_{\rm L}^{\rm GW}}{\partial z}\right| {\rm d}z, \quad (2.11)$$

where $\det(\mathbf{J}_d(z))$ is the determinant of the Jacobian matrix, $\mathbf{J}_d(z)$, of the function $\hat{d}_{\rm L}^{\rm GW}(z)$. Since the integrand in the likelihood 2.10 is a function of $d_{\rm L}^{\rm GW}$, this transform can be applied to rewrite Equation 2.10 as,

$$p(\gamma|x_{\rm GW}, x_{\rm EM}) \propto \iiint p(x_{\rm GW}|\hat{d}_{\rm L}^{\rm GW}(z, \gamma, H_0, \Omega_{\rm m})) p(x_{\rm EM}|z) \\ p(\hat{d}_{\rm L}^{\rm GW}(z, \gamma, H_0, \Omega_{\rm m})|H_0, \Omega_{\rm m}) p(\gamma) p(H_0) p(\Omega_{\rm m}) \frac{\partial d_{\rm L}^{\rm GW}}{\partial z} {\rm d}z {\rm d}H_0 {\rm d}\Omega_{\rm m}. \quad (2.12)$$

Since $\hat{d}_{\rm L}^{\rm GW}$ is the inverse of $\hat{z}$, $\hat{z}(\hat{d}_{\rm L}^{\rm GW}(z)) = z$, and for $z > 0$, $\hat{d}_{\rm L}^{\rm GW}(z)$ is monotonically increasing so $\partial \hat{d}_{\rm L}^{\rm GW}/\partial z$ is strictly positive and hence is equal to its absolute value. Following Pardo et al. [43], a "uniform-in-modified-comoving-volume-time" distance prior is adopted:

$$p(\hat{d}_{\rm L}^{\rm GW}(z, \gamma, H_0, \Omega_{\rm m})|H_0, \Omega_{\rm m}) \propto \frac{1}{1+z} \frac{{\rm d}V_{\rm C}^{\rm GW}}{{\rm d}d_{\rm L}^{\rm GW}} \\ = \frac{1}{1+z} \frac{\partial V_{\rm C}^{\rm GW}}{\partial V_{\rm C}} \frac{\partial V_{\rm C}}{\partial z} \frac{\partial z}{\partial d_{\rm L}^{\rm GW}} \propto p(z|H_0, \Omega_{\rm m}) \frac{\partial V_{\rm C}^{\rm GW}}{\partial V_{\rm C}} \frac{\partial z}{\partial d_{\rm L}^{\rm GW}}, \quad (2.13)$$

where $p(z|H_0, \Omega_{\rm m})$ is the prior on z, described by Equation 2.16 and $V_{\rm C}^{\rm GW}$ is the comoving volume modified to account for gravitational leakage,

$$V_{\rm C}^{\rm GW} = \frac{4\pi}{3} (1+z)^{3\gamma-3} d_{\rm C}^{3\gamma}. \quad (2.14)$$

[8] Note that this would not be the case if 2.10 had a prior on z as $P_{\rm det}^{\rm GW}$ would be a function of γ.

[9] Sampling in $d_{\rm L}^{\rm GW}$ from Equation 2.10 requires inverting Equation 2.4 with respect to z. Practically, this means either using something like `astropy.cosmology`'s `z_at_value` function or setting a cosmology and interpolating 2.4 over a range of z values and inverting it. Both methods are *very* inefficient.

Table 1. Priors used in inference.

	Parameter	Prior
	γ	$\mathcal{U}(0.75, 1.2)$
	z	Uniform-in-comoving-volume-time [33]
Planck 2018 [12]	H_0	$\mathcal{N}(\mu = 67.37, \sigma = 0.54)$ km Mpc^{-1} s^{-1}
	Ω_m	$\mathcal{N}(\mu = 0.3147, \sigma = 0.0074)$
SH$_0$ES 2019 [47]	H_0	$\mathcal{N}(\mu = 74.03, \sigma = 1.42)$ km Mpc^{-1} s^{-1}
	Ω_m	$\mathcal{N}(\mu = 0.30, \sigma = 0.13)$

Finally, substituting 2.13 into Equation 2.12 gives:

$$p(\gamma|x_\mathrm{GW}, x_\mathrm{EM}) \propto \iiint p(x_\mathrm{GW}|\hat{d}_\mathrm{L}^\mathrm{GW}(z, \gamma, H_0, \Omega_\mathrm{m}))p(x_\mathrm{EM}|z) \\ p(z|H_0, \Omega_\mathrm{m})p(\gamma)p(H_0)p(\Omega_\mathrm{m})\frac{\partial V_\mathrm{C}^\mathrm{GW}}{\partial V_\mathrm{C}}\mathrm{d}z\mathrm{d}H_0\mathrm{d}\Omega_\mathrm{m}. \quad (2.15)$$

This is the posterior on γ, expressed as a function of z, H_0, and Ω_m. Sections 2.2 and 2.3 describe the likelihoods and priors used in Equation 2.15 and then Section 2.4 details the methods used to approximate the integral, thus obtaining a posterior distribution for γ.

2.2. *Priors*

The prior distributions used for this analysis are presented in Table 1. For the cosmological parameters, the analysis was performed using Planck 2018 [12] and SH$_0$ES 2019 [47] measurements of H_0 and Ω_m. The difference between these priors isn't enough to meaningfully shift the posterior on γ but it is potentially enough to observe some preference for one or the other, given an expected value of γ, so both are included. For redshift, the uniform-in-comoving-volume-time prior is given by:

$$p(z) \propto \frac{1}{(1+z)}\mathrm{d}V_\mathrm{C} \propto \frac{c}{H_0}\frac{1}{(1+z)^3}\frac{(d_\mathrm{L})^2}{E(z)}\mathrm{d}z\mathrm{d}\Omega, \quad (2.16)$$

where $\mathrm{d}V_\mathrm{C}$ is the comoving volume element with d_L as defined in Equation 1.12. The factor of $1/(1+z)$ accounts for time dilation between events in the observer frame. An uninformative prior is set on γ.

2.3. *The Data*

The source host galaxy redshift and sky-position data is presented in Table 2. Redshift likelihood distributions ($p(x^\mathrm{EM}|z)$ in Equation 2.15) are approximated by Gaussian distributions, $\mathcal{N}(z, \sigma_z^2)(\mu_z)$, centred on z and evaluated at the mean value of z_obs, as in Abbott et al. [5]. Right ascension and declination (α, δ) are fixed. These values are obtained from the Sloan Digital Sky Survey [13] and the NASA/IPAC Extragalactic Database [35].

Table 2. EM data values. Redshift is represented as a mean and standard deviation of an assumed Gaussian distribution.

Source Galaxy	Parameter	Value
NGC 4993 [32][35] (GW170817)	$z_{\rm obs} : \mu_z \pm \sigma_z$	$9.80 \pm 0.79 \times 10^{-3}$
	α	$197.45°$
	δ	$-23.38°$
AGN J1249 + 3449 [13] (GW190521)	$z_{\rm obs} : \mu_z \pm \sigma_z$	0.438 ± 0.00003
	α	$192.43°$
	δ	$34.82°$

The GW data is obtained in the form of samples drawn from the $p(\vec{\theta}|x^{\rm GW})$ posterior distribution from the GW parameter estimation [7, 11] performed on each signal, where $\vec{\theta}$ is the set of GW parameters considered by the model. Posterior samples from the GW170817 parameter estimation are retrieved from Abbott et al. [7], where the analysis was performed with sky-position fixed on the EM source host galaxy, using the waveform model `IMRPhenomPv2 NRTidal`. There is a choice of different posterior samples for GW190521, using different families of waveform models. Effective one-body models approximate the binary as a single body orbiting a stationary black hole, with masses chosen so that the effective energy of the system is the same as that of the two-body problem [17]; phenomenological models use post Newtonian expansions, numerical relativity (NR) and black hole perturbation theory to individually model the inspiral, merger and ringdown respectively, and then overlap and interpolate over the three to create a single waveform [49]; and NR surrogate models interpolate through the parameter space of a bank of NR simulated waveforms to predict new, unsimulated waveforms [25]. The vastly different approaches to the construction of these models and the fact that the analysis of GW190521 requires sampling of parameters outside of the calibration range[10] [53, 42] of all of them [10], means that no single set of results is guaranteed to be any more valid than the others. Hence all three sets of posterior samples are considered in this analysis[11].

Since the EM counterpart for GW190521 is not yet confirmed, there are no published posterior samples with fixed sky-position. This problem was circumvented by Dr. Veitch who performed parameter estimation on GW190521 strain data using `IMRPhenomPv3HM` (IMR) with the same settings described in Abbott et al. [9], with the exception of sky-position fixed on the EM source galaxy and a uniform-in-comoving-volume luminosity distance prior (as opposed to a uniform-in-Euclidean-volume prior).

[10] For example, mass ratio and spin magnitudes.
[11] The extent of the difference between the three models is apparent in the dissimilarity of the distance likelihoods shown in Figure 3.

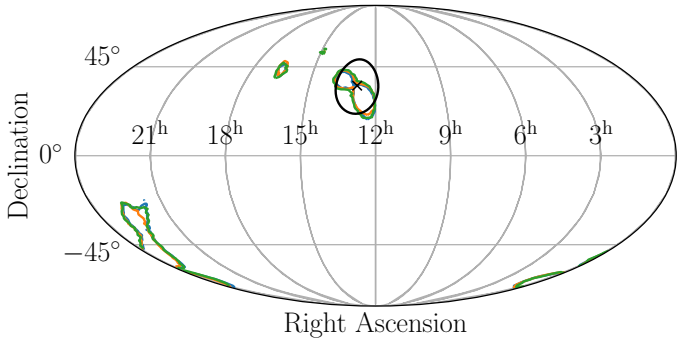

Figure 2. A mollweide projection of a sky map showing the solid angle, outside which posterior samples are discarded, in black. The coloured lines are the 90% probability contours of the three waveform models.

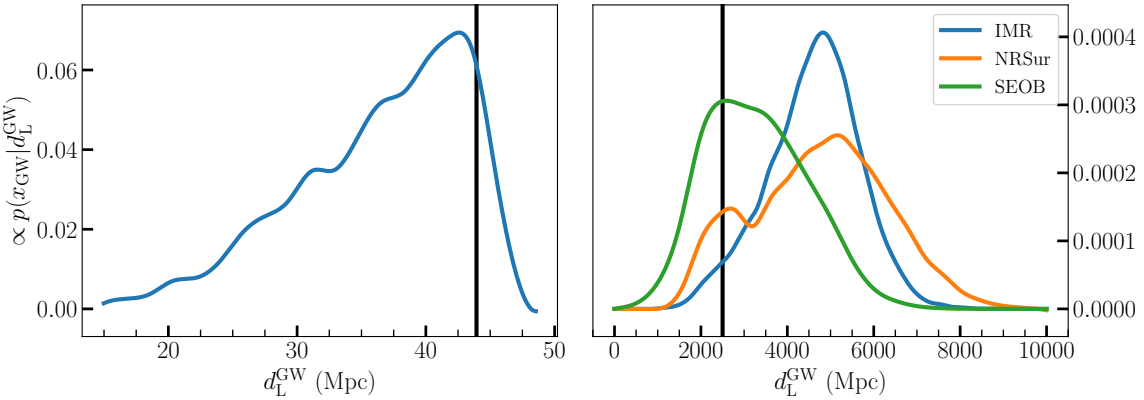

Figure 3. The renormalised distance likelihoods for GW170817 (left) and GW190521 (right). The black lines are the distances to the events given the mean measured redshifts and a Planck 2018 [12] ΛCDM GR cosmology.

Dr. Veitch's posterior samples are used to calibrate a process for discarding samples from the `NRSur7dq4` (NRSur) and `SEOBNRv4PHM` (SEOB) posteriors from Abbott et al. [11] (The Ligo-Virgo Collaboration: LVC) to approximate a fixed sky-position posterior. This ensures the data is as consistent as possible to avoid introducing systematic error to the results. The posteriors are found by selecting samples within an angle θ of the EM source sky-location and discarding the rest. This θ is estimated by comparing Dr. Veitch's posterior samples for IMR to the published LVC results for the same model. For each $\theta_i \in [0.01, \pi]$ radians, LVC samples are discarded and then both the remaining samples and Dr. Veitch's samples are histogrammed into 20 bins, normalised, and a χ^2 value between the two distributions is computed for each bin. For increasing θ_i, the sum over the bins of the χ^2 value is found to fall sharply for $\theta_i < 0.25$ rad and then increase for $\theta_i > 1$ rad. Hence θ is chosen to be 0.25 rad, leaving 6,000–10,000 samples for each waveform model. It is assumed that this value of θ produces a similarly accurate approximation for all models. Figure 2 shows the solid angle with radius θ radians, plotted over the GW190521 sky map. The data

used in the analysis of GW190521 is therefore a combination of selected LVC samples (NRSur and SEOB) and Dr. Veitch's samples (IMR).

An approximation of the marginal $p(d_{\rm L}^{\rm GW}|x^{\rm GW})$ posterior is recovered by creating a 20 bin histogram of the luminosity distance samples, effectively projecting the samples onto the $d_{\rm L}^{\rm GW}$-axis. The distance likelihoods ($p(x^{\rm GW}|d_{\rm L}^{\rm GW})$ in Equation 2.15) for the GW events are then approximated using Bayes theorem by dividing the distance posterior distributions by their respective priors used in the parameter estimation analysis. In the case of all LVC data (GW170817 and GW190521) this is a uniform-in-Euclidean-volume ($\propto (d_{\rm L}^{\rm GW})^2$) prior, and for Veitch's (and Nitz's, see Appendix B) data, this is a uniform-in-comoving-volume prior, with a Planck 2015, ΛCDM cosmology. The resulting luminosity distance likelihoods are presented in Figure 3. The analysis is repeated for the 4 sets of GW distance likelihood, for each set of cosmological priors, for a total of 8 times.

2.4. *MCMC Sampling*

Multidimensional integrals such as the one given in Equation 2.15 can be evaluated using numerical integration but this is a slow and very computationally expensive process. This can be avoided by implementing a stochastic sampling algorithm to approximate the integral [34]. Algorithms like this are designed to draw samples from the parameter space such that areas of high probability are more likely to be sampled, thus allowing the distribution to be reconstructed by creating a histogram of the samples.

The 4-dimensional posterior distribution constructed in Section 2.1 is sampled using `emcee` [29], a Python implementation of an affine-invariant ensemble sampler for Markov chain Monte Carlo (MCMC). The sampler is run for 100,000 samples (of which the first 500 are discarded to account for the burn-in) and 100 walkers. Starting positions for each of the walkers are required by `emcee` so, to ensure they are all within reasonable distance of the mode, a maximal value of the γ posterior is approximated by computing the 1-dimensional posterior along 1000 values of γ, with z, H_0 and $\Omega_{\rm m}$ fixed at their mean values. Walker starting points are then selected by choosing random numbers of the order of σ, the standard deviation for each parameter and distributing them around the mode. This ensures all 100 of the walkers start in an area of non-zero probability.

For each of the 8 combinations of likelihoods and priors, the γ posterior is obtained by histogramming the 100×99,500 γ samples into 45 bins ranging from 0.75 to 1.2, and normalising the resulting distribution. The number of bins is chosen to minimise noise introduced by the binning process, whilst preserving the structure of the distribution. The posterior distributions for GW190521 are combined with those of GW170817 by multiplying the probabilities in the corresponding bins and then renormalising. Posteriors for GW170817, the SEOB model posteriors for GW190521 and the combined GW170817+GW190521 SEOB posteriors are plotted in Figures 4

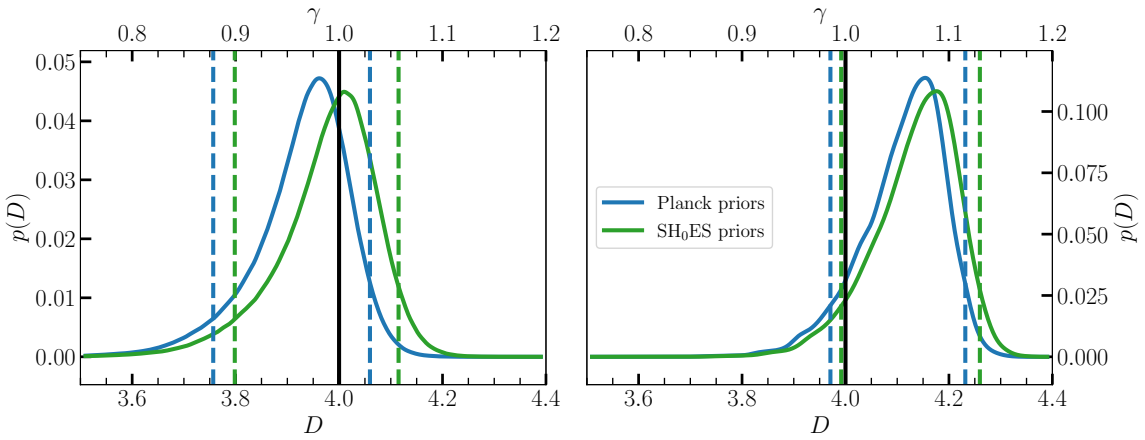

Figure 4. Posterior distributions for γ and D, with Planck (blue) and SH_0ES (green) cosmological priors. The left figure shows the distribution for GW170817 and the right shows GW190521 analysed using the SEOB waveform model. The 90% credible intervals are represented by dashed lines. The black line denotes $\gamma = 1$, corresponding to the GR value of spacetime dimensions $D = 4$.

and 5 in the next section. Constraints on the value of γ from each analysis are also presented in Table 3.

3. RESULTS

The inferred parameters obtained from the inference for each GW event and the combined results are reported in Table 3. They are given as a maximum a posteriori (MAP) with the upper and lower 90% credible interval (CI) values. The plots provided in the main text for GW190521 are all using the SEOB waveform model. The plots for the other models can be found in Appendix A. Each plot shows the interpolated, normalised histogram, described in Section 2, of a single waveform model and the symmetric 90% CI values for each set of priors (Planck or SH_0ES, see Table 1).

The results for GW170817 (Figure 3) agree well with GR. They differ slightly from the results in Pardo et al. [43] which is likely due to updated Planck and SH_0ES measurements[12] and the uniform-in-comoving-volume-time distance prior used here. The GW190521 results "lean" towards higher values of D due to the luminosity distance likelihoods having high support for greater distances. Of the three waveform models, only the SEOB model has $D = 4$ within the 90% CI. The IMR model agrees least, with $D = 4$ lying just outside of 99% CI for the SH_0ES priors. Nevertheless, combining posteriors from both events yields results consistent with GR, within the corresponding 90% CI. The constraints on γ and D are marginally improved for the combined results compared to the GW170817 results alone, in particular the lower bounds are generally improved by a factor of two.

[12] Pardo et al. [43] use the 2015 and 2016 published values whereas this analysis uses the 2018 and 2019 values.

Table 3. Constraints on γ and D. The values presented are the MAP and 90% CI.

Event	Waveform Model	Priors	γ	D
GW170817	IMRPhenomPv2 NRTidal	Planck	$0.98^{+0.05}_{-0.10}$	$3.96^{+0.10}_{-0.21}$
		SH_0ES	$1.00^{+0.05}_{-0.11}$	$4.01^{+0.11}_{-0.21}$
GW190521	IMRPhenomPv3HM	Planck	$1.09^{+0.03}_{-0.05}$	$4.19^{+0.07}_{-0.10}$
		SH_0ES	$1.11^{+0.04}_{-0.05}$	$4.21^{+0.08}_{-0.10}$
	NRSur7dq4	Planck	$1.11^{+0.04}_{-0.08}$	$4.23^{+0.07}_{-0.15}$
		SH_0ES	$1.13^{+0.04}_{-0.08}$	$4.25^{+0.08}_{-0.15}$
	SEOBNRv4PHM	Planck	$1.07^{+0.04}_{-0.09}$	$4.15^{+0.08}_{-0.18}$
		SH_0ES	$1.09^{+0.04}_{-0.09}$	$4.17^{+0.09}_{-0.18}$
Combined GW170817 + GW190521	IMRPhenomPv3HM	Planck	$1.02^{+0.05}_{-0.05}$	$4.05^{+0.10}_{-0.10}$
		SH_0ES	$1.06^{+0.04}_{-0.06}$	$4.11^{+0.08}_{-0.11}$
	NRSur7dq4	Planck	$1.00^{+0.06}_{-0.04}$	$4.01^{+0.13}_{-0.08}$
		SH_0ES	$1.03^{+0.07}_{-0.04}$	$4.05^{+0.13}_{-0.09}$
	SEOBNRv4PHM	Planck	$1.01^{+0.04}_{-0.05}$	$4.01^{+0.09}_{-0.10}$
		SH_0ES	$1.03^{+0.05}_{-0.05}$	$4.05^{+0.10}_{-0.10}$

4. DISCUSSION & CONCLUSIONS

This work presents new results, placing constraints on the number of spacetime dimensions experienced by gravity. Extra-dimensional models of gravity, such as the DGP model, predict that over large distances, gravity should experience "leakage" into these other dimensions, manifesting as a decrease in the amplitude of GW signals from sources beyond a crossing scale, R_c. Here, this deviation is defined in terms of a gravitational leakage parameter, γ. Constraints on γ are inferred from luminosity distance measurements of GW events with detected EM counterparts, from which redshift measurements can be made. For the first, relatively local event, GW170817, the results are found to be in strong agreement with GR but for the distant event, GW190521, results are mixed depending on the waveform model used for the GW parameter estimation. Only the SEOB waveform model yielded results compatible with GR. Combining both events yields results consistent with GR at a 0.1 significance level, with marginally tighter constraints than GW170817 alone.

There is a lot of room for speculation as to why some of the GW190521 results are in disagreement with GR. For one, the assumption that the EM signal associated

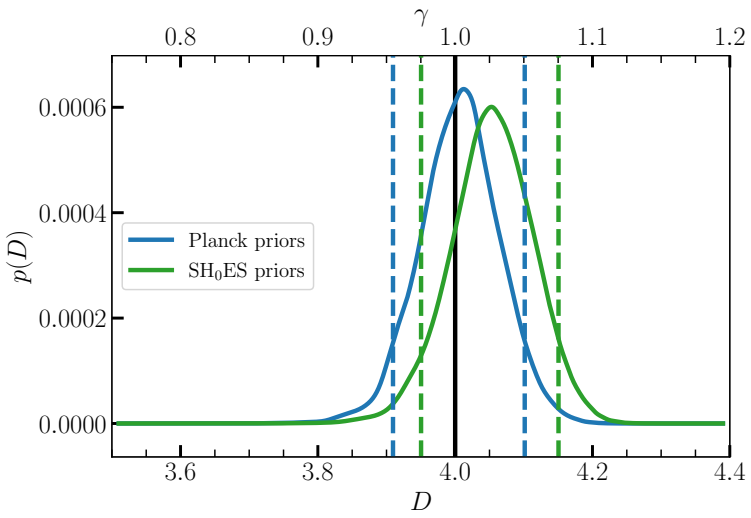

Figure 5. Combined GW170817+GW190521 posterior distribution for γ and D, with Planck (blue) and SH_0ES (green) cosmological priors, for the SEOB waveform model. Posteriors for the other waveform models are plotted in Appendix A. The 90% credible intervals are represented by dashed lines. The black line denotes $\gamma = 1$, corresponding to the GR value of spacetime dimensions $D = 4$

with the event could be false. Ashton et al. [15] propose that there is not sufficient evidence to suggest that the two events are related. According to Graham et al. [31] however, if the flash occurred by their proposed mechanism, the merger recoil kick was not enough for the resultant black hole to escape its AGN and they predict that its orbital path will cause it to reenter the accretion disk within ~ 2 years of the merger, at which time a similar flare can be observed, providing much stronger evidence in favour of their analysis.

There are also difficulties in approximating the signal with the currently available waveform models, due to the need to sample outside of the calibration range of these models to accurately describe the event. This can only be solved by comparing the signal to full NR simulations. For example, Yang et al. [56] perform 325 NR simulations to conclude that the event was most consistent with a highly eccentric merger of two more massive objects at a distance of just 1840^{+1070}_{-540} Mpc. This could potentially place GW190521 closer to its proposed EM counterpart and, although the final mass is higher, it is still consistent with the rough order-of-magnitude estimate performed in Graham et al. [31] to calculate the mass required to produce the accretion disk flare. The assertion by Abbott et al. [11] that both of the individual masses lie within a predicted BH mass gap [26], lends further weight to the argument that the event occurred at a lower luminosity distance than quoted in their analysis. The total mass is better constrained than the individual masses and in order to observe the total mass inferred, the two masses would have to straddle [27] the mass gap, resulting in a lower mass ratio, which in turn produces a "quieter" GW signal. This would suggest that the luminosity distance in Abbott et al. [11] has been overestimated.

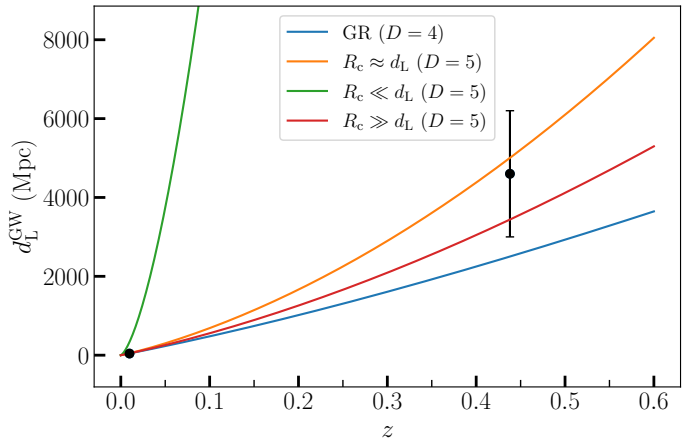

Figure 6. A Hubble diagram demonstrating how the relationship between GW luminosity distance and redshift (solid lines) varies with crossing scale. Black dots are inferred distances from GW events against their EM counterpart redshift with error bars representing a 68% CI.

There is another alternative analysis of GW190521 by Nitz & Capano [41], which considers the possibility of the signal being due to a merger of two bodies with a much lower[13] mass ratio. Since posterior samples from this analysis have been provided, it is possible to repeat the method described here using their results. The results of this, along with a short discussion of their paper, are provided in Appendix B.

While the results may be generally consistent with $(3+1)$-dimensional GR, this is *not* to say that the results are *inconsistent* with higher-dimensional theories. The only case that has been discussed so far is that where $R_c \ll d_L$ but there is no practical reason to assume this other than as an ansatz to facilitate a simple computation. Dvali et al. [22] and Deffayet & Menou [21] both predict that such a R_c should be in the range of d_H–$4d_H \sim 4$–16 Gpc which is in fact more distant than both of the events examined here. Figure 6 is a Hubble diagram which uses Equation 1.7 to plot the inferred gravitational wave luminosity distance, given z, for three different crossing scales[14] for a $(4+1)$-dimensional universe. This demonstrates how GW170817 and GW190521 are consistent both with GR and some 5-dimensional extensions of GR. It is not possible to draw any more concrete conclusions with only two events.

The next few decades are going to be trying for GR as it will have to withstand the rigorous testing of its foundations that occurs with the launch of the space based Laser Interferometer Space Antenna (LISA). LISA will be able to detect transient events up to a redshift of 15 [14] and will be able to perform accurate sky-localisation of sources so that more EM counterparts will be identified, thus populating diagrams like Figure 6. This will allow for curve fitting to further constrain D and its crossover scale and steepness, R_c and n. Corman et al. [20] discuss the potential of LISA to

[13] In their paper [41], Nitz & Capano use the convention that mass ratio, q is defined by m_1/m_2 where $m_1 > m_2$ whereas the standard is to use $q = m_2/m_1$ so that q is in the range $(0, 1]$, thus they would say they present a higher mass ratio, rather than a lower one.

[14] All with transition steepness of $n = 1$, just to keep it simple.

constrain the number of spacetime dimensions and other GR expansion parameters, as well as the cosmological constants, on ranges not yet tested by EM observations.

Code is available at github.com/2335083k/Honoursproject.

REFERENCES

[1]Abbott, B., Abbott, R., Abbott, T., et al. 2017, The Astrophysical Journal, 848, L12, doi: 10.3847/2041-8213/aa91c9

[2]—. 2019, Physical Review X, 9, doi: 10.1103/physrevx.9.031040

[3]—. 2019, Physical Review D, 100, doi: 10.1103/physrevd.100.104036

[4]—. 2019, Physical Review Letters, 123, doi: 10.1103/physrevlett.123.011102

[5]Abbott, B. P., Abbott, R., Abbott, T. D., et al. 2017, Nature, 551, 85–88, doi: 10.1038/nature24471

[6]—. 2017, Phys. Rev. Lett., 119, 161101, doi: 10.1103/PhysRevLett.119.161101

[7]—. 2019, Phys. Rev. X, 9, 011001, doi: 10.1103/PhysRevX.9.011001

[8]—. 2021, The Astrophysical Journal, 909, 218, doi: 10.3847/1538-4357/abdcb7

[9]Abbott, R., Abbott, T. D., Abraham, S., et al. 2020, GWTC-2: Compact Binary Coalescences Observed by LIGO and Virgo During the First Half of the Third Observing Run. https://arxiv.org/abs/2010.14527

[10]Abbott, R., Abbott, T., Abraham, S., et al. 2020, Physical Review Letters, 125, doi: 10.1103/physrevlett.125.101102

[11]Abbott, R., Abbott, T. D., Abraham, S., et al. 2020, The Astrophysical Journal, 900, L13, doi: 10.3847/2041-8213/aba493

[12]Aghanim, N., Akrami, Y., Ashdown, M., et al. 2020, Astronomy & Astrophysics, 641, A6, doi: 10.1051/0004-6361/201833910

[13]Alam, S., Albareti, F. D., Allende Prieto, C., et al. 2015, ApJS, 219, 12, doi: 10.1088/0067-0049/219/1/12

[14]Amaro-Seoane, P., Audley, H., Babak, S., et al. 2017, Laser Interferometer Space Antenna. https://arxiv.org/abs/1702.00786

[15]Ashton, G., Ackley, K., Hernandez, I. M., & Piotrzkowski, B. 2020, Current observations are insufficient to confidently associate the binary black hole merger GW190521 with AGN J124942.3+344929. https://arxiv.org/abs/2009.12346

[16]Bull, P., Akrami, Y., Adamek, J., et al. 2016, Physics of the Dark Universe, 12, 56, doi: https://doi.org/10.1016/j.dark.2016.02.001

[17]Buonanno, A., & Damour, T. 1999, Physical Review D, 59, doi: 10.1103/physrevd.59.084006

[18]Chen, H.-Y., Fishbach, M., & Holz, D. E. 2018, Nature, 562, 545–547, doi: 10.1038/s41586-018-0606-0

[19]Clifton, T., Ferreira, P. G., Padilla, A., & Skordis, C. 2012, Physics Reports, 513, 1–189, doi: 10.1016/j.physrep.2012.01.001

[20]Corman, M., Escamilla-Rivera, C., & Hendry, M. 2021, Journal of Cosmology and Astroparticle Physics, 2021, 005–005, doi: 10.1088/1475-7516/2021/02/005

[21]Deffayet, C., & Menou, K. 2007, The Astrophysical Journal, 668, L143–L146, doi: 10.1086/522931

[22]Dvali, G., Gabadadze, G., & Porrati, M. 2000, Physics Letters B, 485, 208–214, doi: 10.1016/s0370-2693(00)00669-9

[23]Dyson, F. W., Eddington, A. S., & Davidson, C. 1920, A Determination of the Deflection of Light by the Sun's Gravitational Field, from Observations Made at the Total Eclipse of May 29, 1919, Zenodo, doi: 10.1098/rsta.1920.0009

[24]Einstein, A. 1915, Sitzungsber. Preuss. Akad. Wiss. Berlin (Math. Phys.), 1915, 844

[25]Field, S. E., Galley, C. R., Hesthaven, J. S., Kaye, J., & Tiglio, M. 2014, Phys. Rev. X, 4, 031006, doi: 10.1103/PhysRevX.4.031006
[26]Fishbach, M., & Holz, D. E. 2017, The Astrophysical Journal, 851, L25, doi: 10.3847/2041-8213/aa9bf6
[27]—. 2020, The Astrophysical Journal, 904, L26, doi: 10.3847/2041-8213/abc827
[28]Fishbach, M., Gray, R., Hernandez, I. M., et al. 2019, The Astrophysical Journal, 871, L13, doi: 10.3847/2041-8213/aaf96e
[29]Foreman-Mackey, D., Hogg, D. W., Lang, D., & Goodman, J. 2013, Publications of the Astronomical Society of the Pacific, 125, 306–312, doi: 10.1086/670067
[30]Freedman, W. L. 2017, Cosmology at at Crossroads: Tension with the Hubble Constant. https://arxiv.org/abs/1706.02739
[31]Graham, M. J., Ford, K. E. S., McKernan, B., et al. 2020, Phys. Rev. Lett., 124, 251102, doi: 10.1103/PhysRevLett.124.251102
[32]Hjorth, J., Levan, A. J., Tanvir, N. R., et al. 2017, The Astrophysical Journal, 848, L31, doi: 10.3847/2041-8213/aa9110
[33]Hogg, D. W. 1999, arXiv e-prints, astro. https://arxiv.org/abs/astro-ph/9905116
[34]Hogg, D. W., & Foreman-Mackey, D. 2018, The Astrophysical Journal Supplement Series, 236, 11, doi: 10.3847/1538-4365/aab76e
[35]Jet Propulsion Laboratory, C. I. o. T. 2021, NASA/IPAC Extragalactic Database. http://ned.ipac.caltech.edu/
[36]Koren, S. 2020, The Hierarchy Problem: From the Fundamentals to the Frontiers. https://arxiv.org/abs/2009.11870
[37]Loredo, T. J. 2004, AIP Conference Proceedings, doi: 10.1063/1.1835214
[38]Lovelock, D. 1971, Journal of Mathematical Physics, 12, 498, doi: 10.1063/1.1665613
[39]Mandel, I., Farr, W. M., & Gair, J. R. 2019, Monthly Notices of the Royal Astronomical Society, 486, 1086–1093, doi: 10.1093/mnras/stz896
[40]Mastrogiovanni, S., Haegel, L., Karathanasis, C., Magana-Hernandez, I., & Steer, D. A. 2020, Gravitational wave friction in light of GW170817 and GW190521. https://arxiv.org/abs/2010.04047
[41]Nitz, A. H., & Capano, C. D. 2020. https://arxiv.org/abs/2010.12558
[42]Ossokine, S., Buonanno, A., Marsat, S., et al. 2020, Physical Review D, 102, doi: 10.1103/physrevd.102.044055
[43]Pardo, K., Fishbach, M., Holz, D. E., & Spergel, D. N. 2018, Journal of Cosmology and Astroparticle Physics, 2018, 048–048, doi: 10.1088/1475-7516/2018/07/048
[44]Perlmutter, S., Aldering, G., Goldhaber, G., et al. 1999, The Astrophysical Journal, 517, 565–586, doi: 10.1086/307221
[45]Popper, D. M. 1954, ApJ, 120, 316, doi: 10.1086/145916
[46]Pratten, G., García-Quirós, C., Colleoni, M., et al. 2020, Let's twist again: computationally efficient models for the dominant and sub-dominant harmonic modes of precessing binary black holes. https://arxiv.org/abs/2004.06503
[47]Riess, A. G., Casertano, S., Yuan, W., Macri, L. M., & Scolnic, D. 2019, The Astrophysical Journal, 876, 85, doi: 10.3847/1538-4357/ab1422
[48]Riess, A. G., Filippenko, A. V., Challis, P., et al. 1998, The Astronomical Journal, 116, 1009–1038, doi: 10.1086/300499
[49]Santamaría, L., Ohme, F., Ajith, P., et al. 2010, Phys. Rev. D, 82, 064016, doi: 10.1103/PhysRevD.82.064016
[50]Schutz, B. 1986, Nature, 323, 310–311, doi: 10.1038/323310a0
[51]Shapiro, I. I. 1964, PhRvL, 13, 789, doi: 10.1103/PhysRevLett.13.789

[52]Soares-Santos, M., Holz, D. E., Annis, J., et al. 2017, The Astrophysical Journal, 848, L16, doi: 10.3847/2041-8213/aa9059

[53]Varma, V., Field, S. E., Scheel, M. A., et al. 2019, Physical Review Research, 1, doi: 10.1103/physrevresearch.1.033015

[54]Wheeler, J. A., & Ford, K. W. 1998, Geons, Black Holes, and Quantum Foam: A Life in Physics, Macmillan Publishers Limited. All rights reserved

[55]Will, C. M. 2014, Living Reviews in Relativity, 17, doi: 10.12942/lrr-2014-4

[56]Yang, Y., Gayathri, V., arka, S. M., arka, Z. M., & Bartos, I. 2020, Determining the Hubble Constant with Black Hole Mergers in Active Galactic Nuclei. https://arxiv.org/abs/2009.13739

APPENDIX

A. ADDITIONAL RESULTS FIGURES

This section presents the γ-D posterior distributions described in Section 3. Also included is a corner plot for GW170817 with Planck priors. Since this plot is not very informative beyond demonstrating an anticorrelation between γ and z, and all of these 8 plots are very similar, the others are not included.

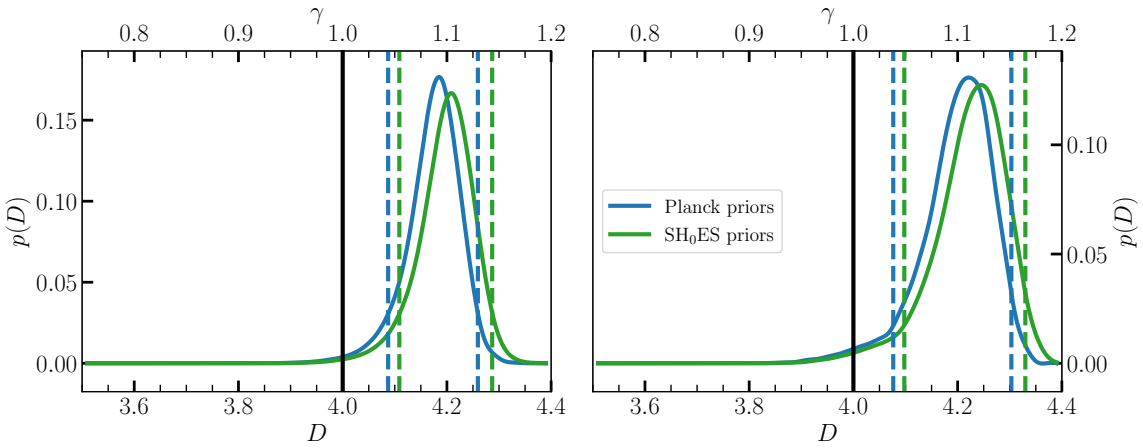

Figure 7. Posterior distributions for γ and D from GW190521, with Planck (blue) and SH_0ES (green) cosmological priors. The left figure shows the distribution for the IMR waveform model and the right shows the NRSur waveform model, and 90% credible intervals are represented by dashed lines.

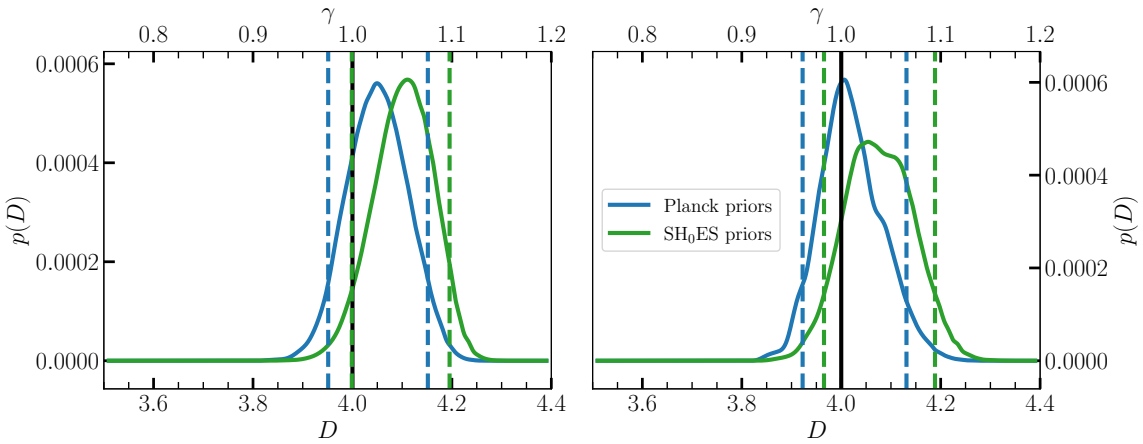

Figure 8. Combined event posterior distributions for γ and D, with Planck (blue) and SH_0ES (green) cosmological priors. The left figure shows the distribution for the IMR waveform model and the right shows the NRSur waveform model. The 90% credible intervals are represented by dashed lines.

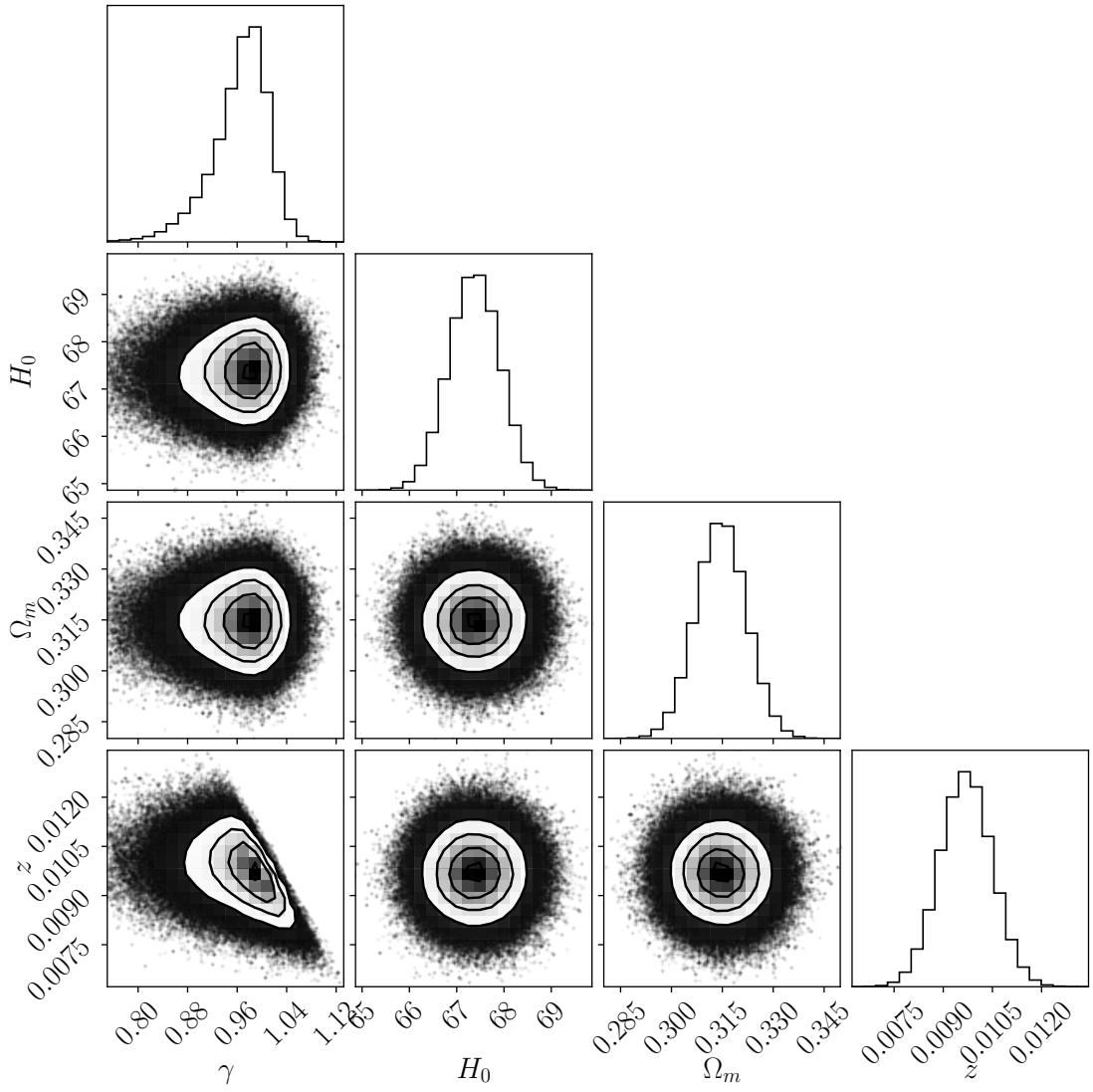

Figure 9. A corner plot showing the 1 and 2-dimensional posteriors for GW170817 with Planck priors. An anticorrelation between γ and z is apparent.

B. NITZ & CAPANO 2020

The paper by Nitz & Capano [41] provides an alternative parameter estimation of GW190521 and hence a different set of luminosity distance posterior samples with which to perform the analysis described in this paper. The inferred distance posteriors differ in several ways, which are detailed in Nitz & Capano [41]. Firstly, the mass priors used here are uniform in mass ratio as opposed to individual masses, as in Abbott et al. [11]. This is to ensure a weighting of the masses that disfavours masses within the mass gap [26]. The distance prior is uniform-in-comoving-volume rather than Euclidean volume but this should not affect the results here as it is the likelihood and not posterior distribution that is required, and hence the prior is factored out. A newer phenomenological waveform model (`IMRPhenomXPHM` [46]) is used

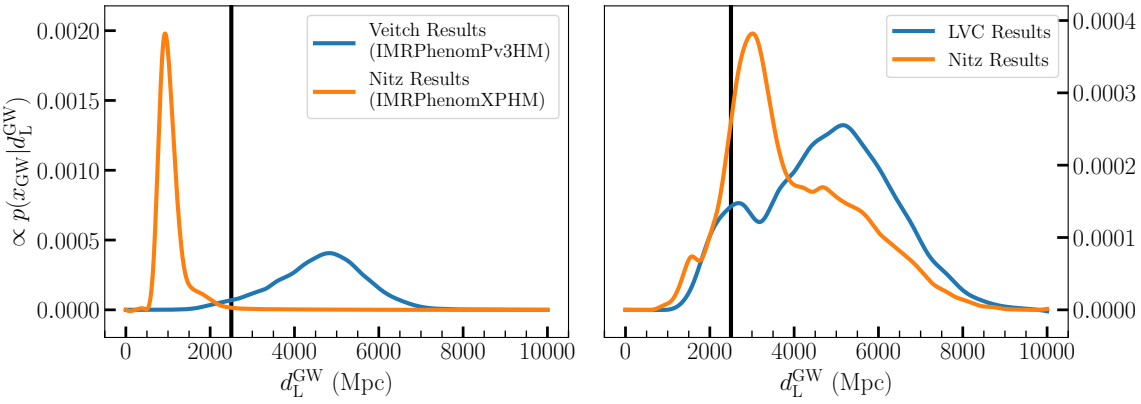

Figure 10. Comparisons of the distance likelihoods obtained by LVC and Nitz & Capano [41] with different mass ratio priors. The likelihoods on the left and right were obtained using the NRSur waveform model and IMR models respectively.

in the Nitz and Capano paper, which is calibrated for lower mass ratios (to q $\approx$ 0.04) and accounts for precession, as well as sub-dominant harmonic modes. They also perform the analysis for the same NRSur model used by LVC for comparison. Finally, they numerically marginalise over the polarization angle and coalescence phase instead of using stochastic sampling to evaluate the entire multidimensional posterior distribution.

They report that their resulting posterior distribution has a bimodal structure for both models. The secondary (higher mass ratio) mode is consistent with the results published by [11]. For the `IMRPhenomXPHM` waveform model, the mass ratio is found to be $q = 0.09$ which is lower than any of the models used in the LVC analysis are capable of sampling [25, 42].

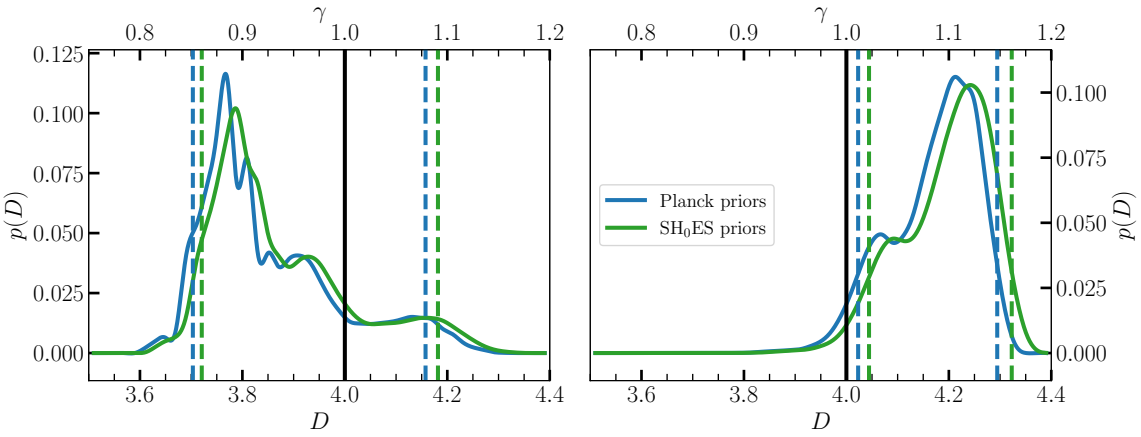

Figure 11. Posterior distributions for γ and D from GW190521, with Planck (blue) and SH_0ES (green) cosmological priors. The left figure shows the distribution for the IMR waveform model and the right shows the NRSur waveform model, and 90% credible intervals are represented by dashed lines.

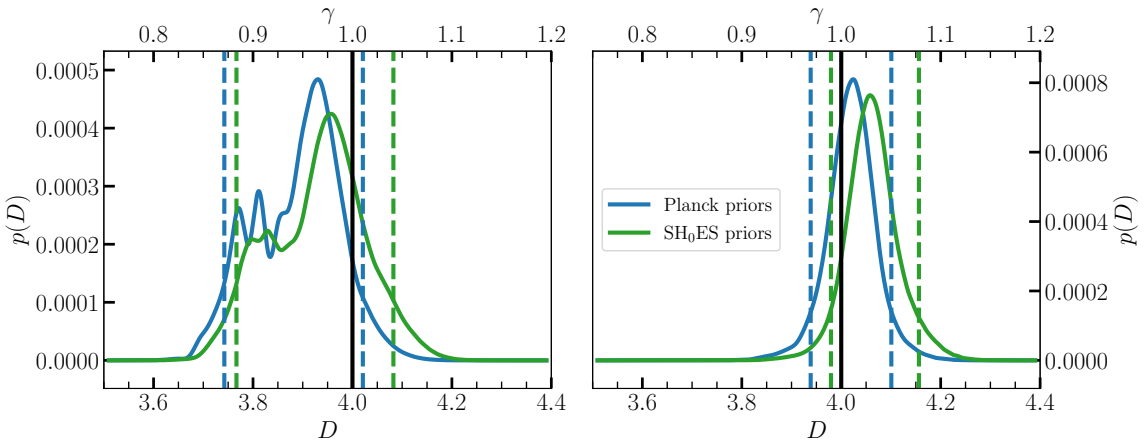

Figure 12. Combined event posterior distributions for γ and D, with Planck (blue) and SH_0ES (green) cosmological priors. The left figure shows the distribution for the IMR waveform model and the right shows the NRSur waveform model, and 90% credible intervals are represented by dashed lines.

The distance likelihoods (recovered from the Nitz posterior samples as described in Section 2.3) are presented in Figure 10 along with the equivalent LVC distance likelihoods for comparison. As is apparent, the lower mass ratio provides strong support for much lower luminosity distances. This is clearer in the IMR waveform model plot as the NRSur model is only calibrated for $q > 0.25$ and hence the primary (lower mass ratio) mode is cut off at this limit.

The results of the parameter estimation described in Section 2 are presented in Table 4 and the posterior γ distributions are plotted in Figures 11 and 12. The jagged shape of the γ posteriors for the IMR model is an artifact of the histogramming of the distance posterior samples. The wide range of distance values combined with the very narrow mode makes it difficult to approximate and results in steps in the distribution which are amplified by the relationship between $d_{\rm L}^{\rm GW}$ and γ. This could be avoided by either sorting the samples into more bins or cutting off the distribution at some point above 2000 Mpc where the probability is very low compared to the peak. Although it is the MAP values that are presented in Table 4 to allow for easier comparison with Table 3, the median is possibly more informative for multimodal distributions such as these. Consequently, the median values are also presented in Table 5.

For GW190521 alone, IMR results are consistent with GR whereas the NRSur results are similar to the LVC results with a slightly different shape. For both models, the combined GW170817+GW190521 results are consistent with (3+1)-dimensional GR at a 90% confidence level.

Table 4. Constraints on γ and D. Alternative results using analysis by Nitz & Capano [41]. As with main results, the values presented are the MAP and 90% CI.

Event	Waveform Model	Priors	γ	D
GW190521	IMRPhenomXPHM	Planck	$0.89^{+0.19}_{-0.03}$	$3.77^{+0.39}_{-0.07}$
		SH_0ES	$0.90^{+0.20}_{-0.03}$	$3.79^{+0.39}_{-0.07}$
	NRSur7dq4	Planck	$1.11^{+0.04}_{-0.09}$	$4.21^{+0.08}_{-0.19}$
		SH_0ES	$1.13^{+0.04}_{-0.10}$	$4.25^{+0.07}_{-0.21}$
Combined GW170817 + GW190521	IMRPhenomXPHM	Planck	$0.97^{+0.05}_{-0.09}$	$3.93^{+0.09}_{-0.19}$
		SH_0ES	$0.98^{+0.06}_{-0.10}$	$3.96^{+0.13}_{-0.19}$
	NRSur7dq4	Planck	$1.01^{+0.04}_{-0.04}$	$4.02^{+0.08}_{-0.09}$
		SH_0ES	$1.03^{+0.05}_{-0.04}$	$4.06^{+0.10}_{-0.08}$

Table 5. Median values for γ and D. Alternative results using analysis by Nitz & Capano [41]. Missing entries indicate that median=MAP.

Event	Waveform Model	Priors	γ	D
GW190521	IMRPhenomXPHM	Planck	0.91	3.82
		SH_0ES	0.92	3.84
	NRSur7dq4	Planck	1.10	4.20
		SH_0ES	1.11	4.22
Combined GW170817 + GW190521	IMRPhenomXPHM	Planck	0.95	3.90
		SH_0ES	0.97	3.94
	NRSur7dq4	Planck	—	—
		SH_0ES	—	—

C. STATEMENT OF WORK

This project was performed almost entirely by myself. Dr. Veitch kindly ran some parameter estimation for me (see Section 2.3) and also offered a considerable amount of support, as well as consultation. Other than this, all planning, record keeping, research and execution are my own work. The idea for the project was my own, inspired by Pardo et al. [43] and heavily based on the work of Deffayet & Menou [21]. I had already planned this project before Mastrogiovanni et al. [40] was published! They beat me to it.

As I have discussed with Professor Woan, I (along with another student, Student Z) completed the bulk of the project in the first semester to avoid timetable clashes

and did not attend the second semester lab sessions. At the end of our 9 lab sessions with Dr. Veitch, we prepared a document to provide him with feedback on his lab and I hope that this has contributed to the experience of our classmates who have chosen the GW project in second semester.

Student Z has been an indispensable as a source of moral support and reassurance, and as a sounding board who has spent many many hours listening to me trying to get my head around Bayesian inference. They also have an incredible gift for explaining concepts and without them I probably would not have been able to understand half of what has gone into this report. They were also kind enough to proof read my report, along with another student.

In addition to the `emcee` analysis described in Section 2.4, I repeated the sampling with a parallel tempering sampler designed by Student Z. It worked comparably well to `emcee` for my purposes, if a little slow!

D. ACKNOWLEDGEMENTS

I would like to credit the lecturers of all of my A345 courses this year: Dr. Hammond, Dr. Hannah, Dr. Gray, Dr. Messenger, Dr. Labrosse and Prof. Hendry, for supplying me with almost all the of the knowledge required to complete this project. In particular, I would like the thank Prof. Hendry for taking the time answer my questions about extra-dimensional gravity and for introducing me to the wonderful paper by Corman et al. [20]. I would again like to emphasise how fantastic Dr. Veitch has been as a supervisor; he has gone above and beyond to be encouraging and supportive, and has introduced me to innumerable interesting ideas (my bookmarks are full of Alcubierre drives and Buckingham π theorems). It has been an absolute pleasure working with him and Student Z.